# Polymerization of Olefins Through Heterogeneous Catalysis IV. Modeling of Heat and Mass Transfer Resistance in the Polymer Particle Boundary Layer

S. FLOYD, K. Y. CHOI, T. W. TAYLOR, and W. H. RAY,*
*Department of Chemical Engineering, University of Wisconsin, Madison, Wisconsin 53706*

## Synopsis

Propylene and ethylene polymerization in liquid and gas media are described by a multigrain particle model. External boundary layer heat and mass transfer effects are investigated for various catalysts and operating conditions. For high-activity catalysts used in slurry, external film mass transfer effects may be significant. For gas-phase polymerization of propylene or ethylene, the model predicts significant particle overheating at short times, which may explain the particle sticking and agglomeration problems sometimes observed in industrial reactors.

## INTRODUCTION

In the previous paper in this series (Part III,[1]), detailed modeling equations for the multigrain model were introduced together with typical operating conditions and parameters for olefin polymerization over a Ziegler-Natta catalyst. The thrust of the previous paper was to develop quantitative criteria for the existence of significant intraparticle concentration and temperature gradients in the growing polymer particle.

The goal of the present paper is to analyze heat and mass transfer resistances in the external boundary layer of the polymer particles. We examine both slurry and gas-phase polymerization reactors and illustrate the results for both ethylene polymerization and propylene polymerization. The effects of catalyst activity, catalyst particle size, and reactor type will be illustrated.

## MASS TRANSFER IN THE PARTICLE BOUNDARY LAYER

It is normally assumed[2-4] that mass transfer coefficients in the external boundary layer are sufficiently large that mass transfer resistance is negligible, so that the monomer concentration at the particle surface $M_S$ is essentially the same as the value in the bulk fluid $M_b$. However, as we shall show here, this conclusion is not always valid for high-activity catalysts, especially for liquid slurry polymerization.

In order to determine whether there is significant mass transfer resistance in the external boundary layer, one may calculate the monomer concentration driving force $\Delta M$ necessary to provide monomer at the observed overall reaction rate $R_{ob}$ (g/g-cat-h). From arguments similar to those employed in determining the time scale for the transients of the intraparticle

* To whom correspondence should be addressed.

Journal of Applied Polymer Science, Vol. 31, 2231–2265 (1986)
 CCC 0021-8995/86/072231-35$04.00

resistances, it is justifiable to make the quasi-steady-state approximation for the external film resistances. The quasi-steady-state mass balance across the external film of the particle is

$$k_s A_p \, \Delta M = \rho_c V_c \frac{R_{ob}}{\mathrm{MW}} \tag{1}$$

where $k_s$ is the external film mass transfer coefficient, $A_p$ is the external surface area of the polymer particle, $\rho_c V_c$ is the initial mass of catalyst in the original catalyst particle of radius $R_c$ and density $\rho_c$, and MW is the molecular weight of the monomer. Thus the required external boundary layer driving force is

$$\Delta M = \frac{\rho_c R_c^3 R_{ob}}{3 k_s R_p^2 \mathrm{MW}} \tag{2}$$

In order to use this expression to assess the effect of external boundary layer mass transfer for a given particle-fluid system, the mass transfer coefficient $k_s$ must be estimated.

## Liquid Slurry Polymerization

For polymerization in liquid slurry, the correlations that seem most appropriate for estimation of $k_s$ are listed as follows:

1. Mass transfer coefficient for a single sphere in a stagnant fluid medium:

$$\mathrm{Sh} = 2 \tag{3}$$

where $\mathrm{Sh} = k_s d_p / D_b$ is the Sherwood number. This estimate of $k_s$ assumes *no* relative motion between the fluid and particle. However, it provides a very conservative lower bound on $k_s$.

2. Ranz-Marshall correlation[5] for a single sphere moving with relative velocity $u$:

$$\mathrm{Sh} = 2 + 0.6 \mathrm{Sc}^{1/3} \mathrm{Re}^{1/2} \tag{4}$$

where $\mathrm{Sc} = \mu / \rho_d D_b$ is the Schmidt number and

$$\mathrm{Re} = \frac{\rho_d u d_p}{\mu} \text{ is the Reynolds number.}$$

3. Calderbank-Jones correlation[6] for agitated slurry reactors:

$$k_s = 0.31 \left( \frac{g_c \mu \, \Delta\rho}{\rho_d^2} \right)^{1/3} \mathrm{Sc}^{-2/3} \tag{5}$$

which has been used by others[7] to estimate $k_s$.

4. Brian-Hales correlation[8]:

$$\mathrm{Sh} = (4 + 1.21\ \mathrm{Pe}^{2/3})^{1/2} \tag{6}$$

where

$\mathrm{Pe} = d_p\mu/D_b$ is the Peclet number.

This correlation was obtained by numerical solution of Stoke's equation.

5. Nelson-Galloway correlation[9]

$$\mathrm{Sh} = \frac{2\zeta + \left\{\dfrac{2\zeta^2(1-\epsilon)^{1/3}}{[1-(1-\epsilon)^{1/3}]^2} - 2\right\}\tanh\zeta}{\left[\dfrac{\zeta}{1-(1-\epsilon)^{1/3}} - \tanh\zeta\right]} \tag{7}$$

where

$$\zeta = [(1-\epsilon)^{-1/3} - 1]\frac{\alpha}{2}\,\mathrm{Re}^{1/2}\,\mathrm{Sc}^{1/3} \tag{8}$$

In order to use correlations 2 through 5, one must determine the fluid/solid relative velocity $u$. From physical reasoning, one might assume that the relative velocity of particle and fluid is roughly that of free fall due to gravity but that the mass transfer would be enhanced by turbulence induced by mechanical agitation and by rising bubbles. However, it has been found experimentally that the actual value of the mass transfer coefficient is at most eight times larger than the value calculated for free-fall conditions.[10] For spherical particles, the terminal velocity for free settling is given as[11]

$$u_t = \begin{cases} \dfrac{g_c d_p^2 \Delta\rho}{18\mu} & \text{for} \quad \mathrm{Re} < 0.4 \\ \left(\dfrac{4g_c{}^2(\Delta\rho)^2}{225\rho_d\mu}\right)^{1/3} d_p & \text{for} \quad 0.4 < \mathrm{Re} < 500 \\ \left(\dfrac{3.1 g_c d_p \Delta\rho}{\rho_d}\right)^{1/2} & \text{for} \quad 500 > \mathrm{Re} \end{cases} \tag{9}$$

It should be noted that the above correlation for terminal velocity is strictly valid only for free-settling conditions. When "hindered settling" conditions are encountered, as will be the case for industrial slurry reactors operating above 40% solids loading, the terminal velocity of the particles could be considerably less than calculated by eq. (9). Oldshue[12] provides a graphic guideline by which one may easily determine whether one is in the hindered settling regime.

Except where indicated, our calculations have assumed a solids fraction of 0.3, which is close to the borderline between the regimes. Thus, using the terminal velocity from eq. (9) should give a reasonable estimate of Re. Furthermore, since the liquid-solid mass transfer coefficient does not depend strongly on power input as long as the solids inventory is suspended,[13] we may consider that the conclusions obtained using these mass transfer coefficient values will be applicable to industrial slurry reactors.

Figure 1 shows Sherwood numbers predicted for propylene slurry polymerization as a function of particle Re number, using several mass transfer correlations with the velocities determined from eq. (9). The physical parameters used in these calculations are tabulated in Table I of Part III.[1] Although diluent viscosity was assumed in the calculations, highly concentrated slurry viscosity effects might reduce $k_s$ by as much as 50%. For the Brian-Hales correlation, the diameter of the initial catalyst particle was 60 $\mu$m (0.006 cm). The values of Sh correspond to the mass transfer coefficients $k_s$ shown in Fig. 2 as a function of polymer particle size. Note that the mass transfer coefficients are large initially but decrease rapidly with particle growth. As expected, the limiting case Sh = 2 gives the lowest value of $k_s$ and the other correlations shown yield similar values. The concentration driving force, $\Delta M$ (mol/L), calculated by these correlations and eq. (2) is shown in Fig. 3 for propylene slurry polymerization with a high activity catalyst ($R_{ob}$ = 4000 g/g-cat/h). It is seen that correlations 2, 3, and 4 give similar predictions. The initial driving force required is about 0.5 mol/L, but this decreases rapidly with particle growth because of the increase in external surface area for mass transfer. In the analysis below, we will use the Ranz-Marshall correlation to determine $k_s$ except where otherwise noted.

The effect of initial catalyst size $d_c$ on the concentration driving force $\Delta M$ required is illustrated in Fig. 4 for a high-activity ($R_{ob}$ = 4000 g/g-cat-h) and a low-activity ($R_{ob}$ = 400 g/g-cat-h) catalyst. Note that the initial $\Delta M$ value can be as large as 1 mol/L when a high-activity catalyst with 100-

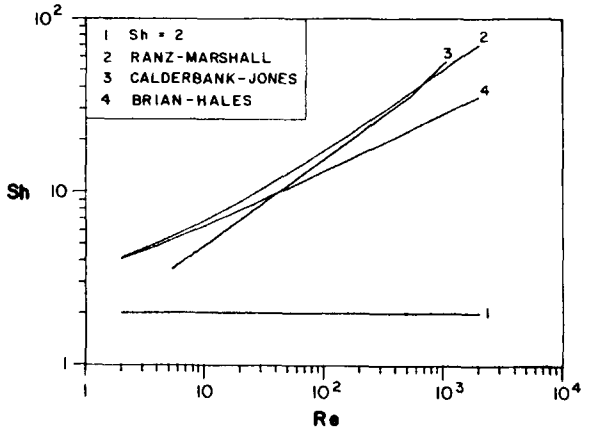


Fig. 1. Comparison of correlations for the Sherwood number for external film mass transfer in propylene slurry polymerization. For Calderbank-Jones correlation an initial particle size of 60 $\mu$m was used.

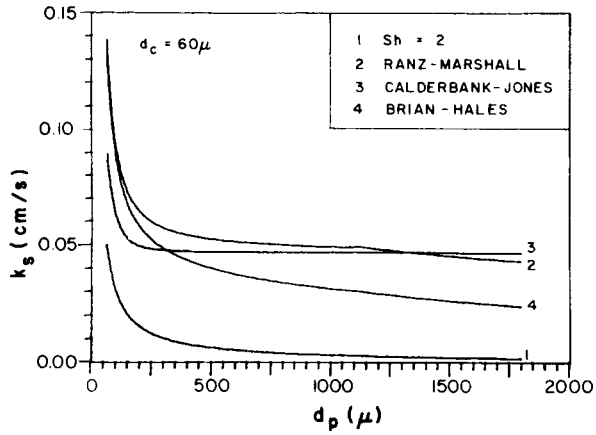


Fig. 2. Mass transfer coefficients from various correlations. Propylene slurry polymerization with initial catalyst particle size of 60 μm.

μm particle diameter is used. In many industrial propylene slurry processes, the concentration of dissolved monomer in the bulk liquid phase is 4 mol/L or more. Thus for the worst case of a highly active catalyst with large catalyst particle size, a significant external mass transfer resistance might be present early in the polymerization. In most cases, however, these effects would be negligible for liquid slurry propylene polymerization.

For ethylene polymerization in slurry, Fig. 5 shows the $k_s$ values as a function of particle size for the various mass transfer correlations. As expected, the values are virtually indistinguishable from those for propylene polymerization (see Fig. 2). Figure 6 shows the external mass transfer resistance for the various correlations. The effect of initial catalyst size for ethylene polymerization is shown in Fig. 7 using the Ranz-Marshall correlation. For large particles of high-activity catalyst, a fairly significant external boundary layer mass transfer resistance may exist in the initial

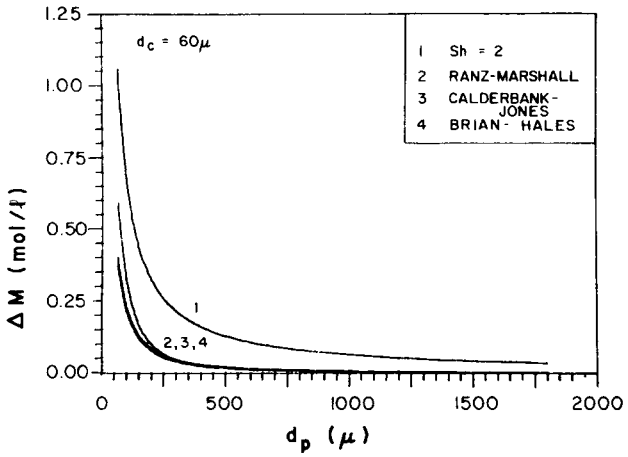


Fig. 3. External film mass transfer resistance in propylene slurry polymerization using various correlations. High-activity catalyst ($R_{ob}$ = 4000 g-g-cat-h) with initial particle size of 60 μm.

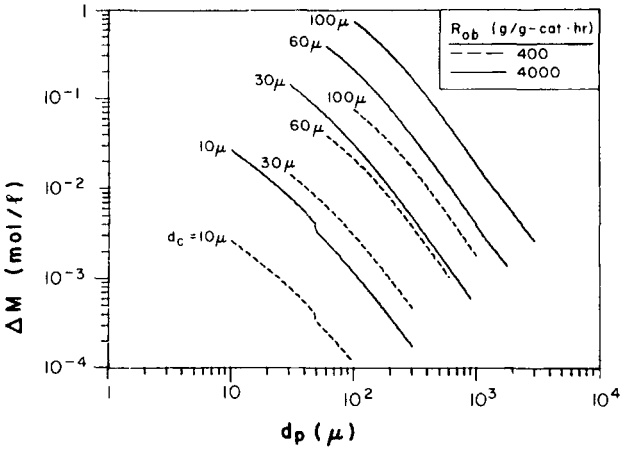


Fig. 4. External film mass transfer resistance in propylene slurry polymerization as a function of polymer particle size using the Ranz-Marshall correlation for low ($R_{ob}$ = 400 g-g-cat-h) and high ($R_{ob}$ = 4000 g-g-cat-h) activity catalysts with various catalyst particle sizes.

stages of particle growth for ethylene polymerization. Moreover, as shown in Table I of Part III, the concentration of dissolved ethylene in industrial slurry polymerization is less than that of propylene. Thus external film mass transfer effects should be more significant for ethylene slurry polymerization than for propylene slurry polymerization.

In contrast to the Ranz-Marshall correlation, which predicts Sherwood numbers of 2 or greater, the Nelson-Galloway correlation predicts Sh considerably less than 2 at low Reynolds numbers. Although, for reasons discussed below, we consider the correlations that predict Sh > 2 to be most appropriate, it is nevertheless instructive to compare the predictions of the Ranz-Marshall correlation with those of the Nelson-Galloway. Figure 8 illustrates the predicted values of $k_s$ for ethylene and propylene slurry polymerization with an initial catalyst particle size of 60 μm. As can be seen here, at high solids concentrations, the Nelson-Galloway correlation predicts a considerable reduction in $k_s$ below the values predicted for low solids loadings (where the two correlations give the same results). For 10-μm

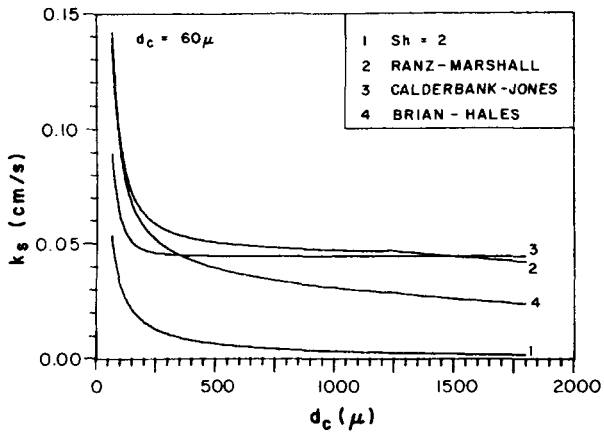


Fig. 5. Mass transfer coefficients from various correlations. Ethylene slurry polymerization with initial catalyst particle size of 60 μm.

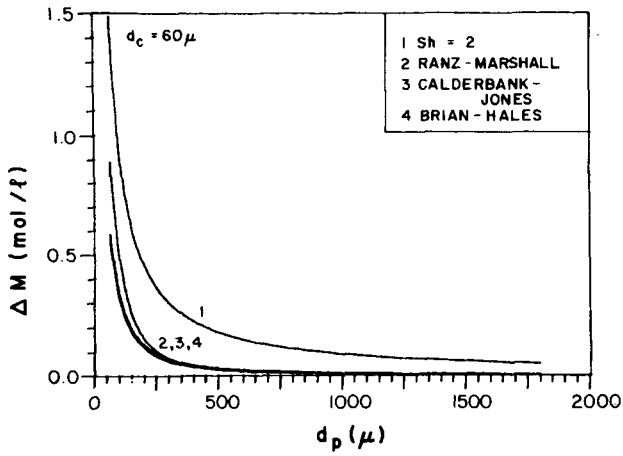


Fig. 6. External film mass transfer resistance in ethylene slurry polymerization with initial catalyst particle size of 60 μm.

catalyst particles, this deviation is even greater, as illustrated in Fig. 9, with predicted $k_s$ values up to three orders of magnitude below those for the Ranz-Marshall correlation. This is primarily due to the break in the particle velocity correlation. One should bear in mind that there is considerable uncertainty inherent in these predictions because of the assumptions of fluid properties, particle apparent density, the precise transition to Stokes flow, and others. Figure 10 shows the predicted mass transfer resistance in propylene slurry polymerization with various catalyst particle sizes, where mass transfer resistances as high as 1 mol/L are predicted for high-activity catalyst in the early stages of polymerization. For ethylene polymerization, Fig. 11 shows that this effect is even more serious. However, it is not clear that the unusual results predicted by the Nelson-Galloway correlation for 10-μm particles are realistic. In any case, it should be noted that the significance of the external film mass transfer resistance is confined to the very early stages of particle growth, even when the Nelson-Galloway correlation is employed.

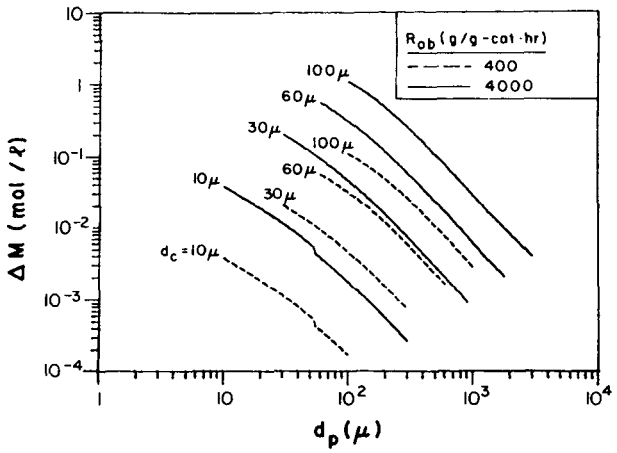


Fig. 7. External film mass transfer resistance in ethylene slurry polymerization as a function of polymer particle size using the Ranz-Marshall correlation for low ($B_{ob}$ = 400 g-g-cat-h) and high ($R_{ob}$ = 4000 g-g-cat-h) activity catalysts with various catalyst particle sizes.

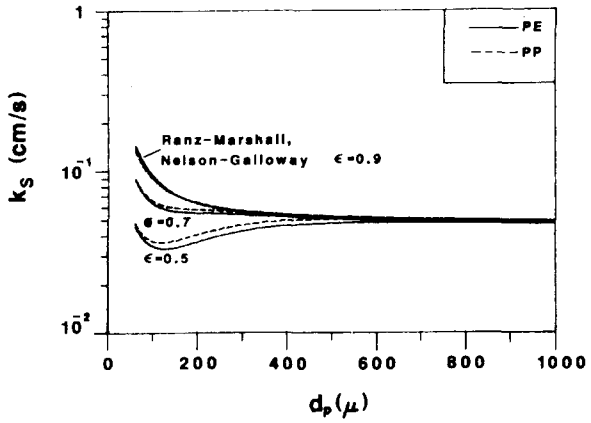


Fig. 8. Mass transfer coefficients according to the Ranz-Marshall and Nelson-Galloway correlations. Ethylene and propylene slurry polymerization with initial catalyst particle size of 60 μm.

Let us now consider mass transfer during abnormal operation. Under certain circumstances during the operation of slurry reactors, it is not inconceivable that agitation could be inadequate for solids suspension or that the agitator could malfunction. Should this occur, the polymerization may be envisioned as taking place in essentially stagnant fluid. The expected mass transfer resistance for such a situation can be predicted by the stagnant limit Sh = 2. Figure 12 illustrates the predicted mass transfer resistance for propylene polymerization for various particle sizes, and Fig. 13 illustrates the case for ethylene slurry polymerization. As seen from these figures, in this special circumstance, a very significant mass transfer resistance is predicted for high-activity catalyst. In fact, for ethylene polymerization with catalysts of large particle size, external film as well as intraparticle mass transfer resistance could drastically limit the reaction rate.

The conclusion one may draw from this analysis is that for slurry poly-

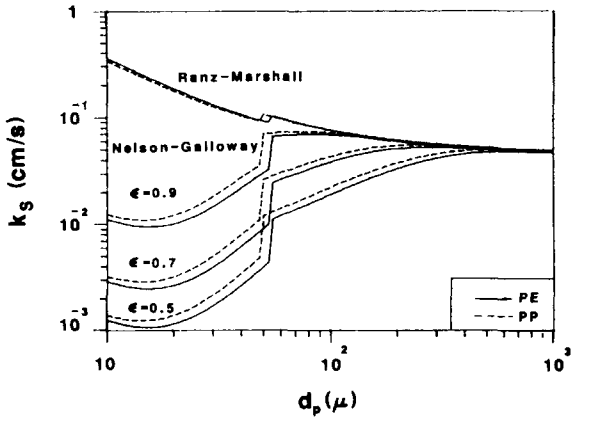


Fig. 9. Mass transfer coefficients according to the Ranz-Marshall and Nelson-Galloway correlations. Ethylene and propylene slurry polymerization with initial catalyst particle size of 10 μm.

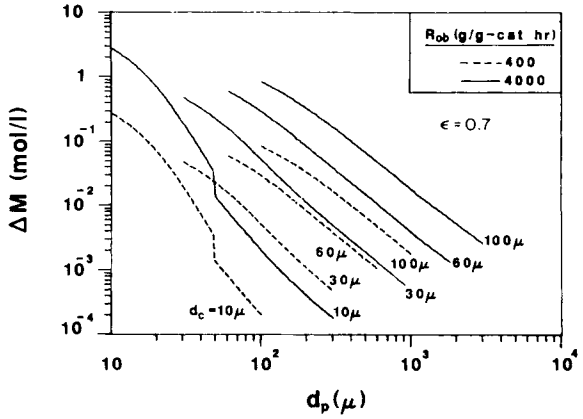


Fig. 10. External film mass transfer resistance in propylene slurry polymerization as a function of polymer particle size using the Nelson-Galloway correlation ($\epsilon = 0.7$) for low ($R_{ob}$ = 400 g-g-cat-h) and high ($R_{ob}$ = 4000 g-g-cat-h) activity catalysts with various catalyst particle sizes.

merization external film mass transfer resistance is only significant early in the polymerization with large particles of high-activity catalyst. However, the external film mass transfer resistance will be more significant for ethylene slurry polymerization than for propylene slurry polymerization.

## Gas-Phase Polymerization

For gas-solid mass transfer, a chaos of correlations, statements, and conclusions are found in the literature, because of the complicated flow characteristics that make experiments difficult to perform.[14-16] In the next section we shall discuss some controversial questions that arise at low Re. Two correlations we shall use are as follows.

1. Ranz-Marshall correlation[17] for a single sphere, which was used previously for liquid phase particle-fluid mass transfer:

$$\mathrm{Sh} = 2 + 0.6\mathrm{Sc}^{1/3}\mathrm{Re}^{1/2} \tag{10}$$

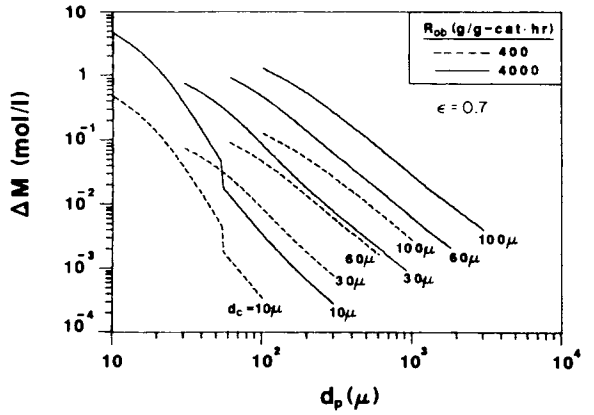


Fig. 11. External film mass transfer resistance in ethylene slurry polymerization as a function of polymer particle size using the Nelson-Galloway correlation ($\epsilon = 0.7$) for low ($R_{ob}$ = 400 g-g-cat-h) and high ($R_{ob}$ = 4000 g-g-cat-h) activity catalysts with various catalyst particle sizes.

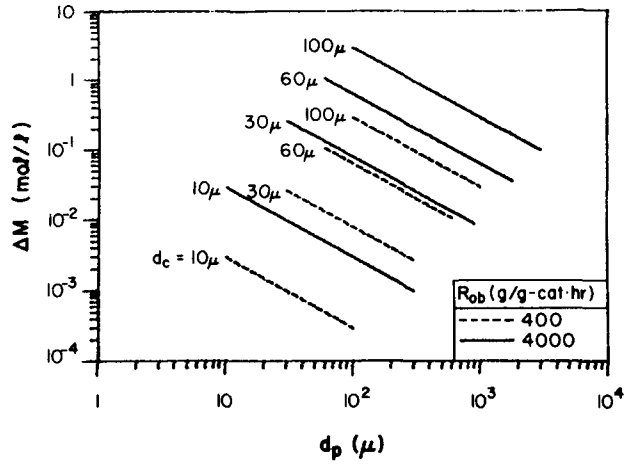


Fig. 12. External film mass transfer resistance in propylene slurry polymerization under stagnant fluid conditions (Sh = 2) as a function of polymer particle size for low ($R_{ob}$ = 400 g-g-cat-h) and high ($R_{ob}$ = 4000 g-g-cat-h) activity catalysts.

2. Richardson-Szekely[18] correlation for shallow gas-fluidized beds. Richardson and Szekely measured mass transfer coefficients by unsteady-state adsorption of carbon tetrachloride vapor from fluidizing air. Their correlation is represented by

$$\begin{aligned} \mathrm{Sh} &= 0.374\mathrm{Re}^{1.18} \quad \text{for} \quad 0.1 < \mathrm{Re} < 15 \\ \mathrm{Sh} &= 2.01\mathrm{Re}^{0.5} \quad \text{for} \quad 15 < \mathrm{Re} < 250 \end{aligned} \tag{11}$$

In order to use these correlations, one must again assume a relative gas velocity for the particle. For stirred bed polymerization reactors Wisseroth[19] quotes a value of $u$ = 1.5 cm/s; for fluidized beds the minimum fluidization velocity is in the range 2–4 cm/s.[17] Except where noted we assume $u$ = 2 cm/s in our calculations.

We should point out again that for homopolymerization with only pure

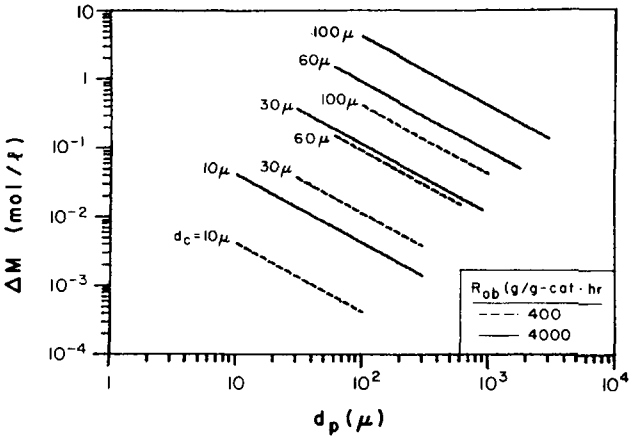


Fig. 13. External film mass transfer resistance in ethylene slurry polymerization under stagnant fluid conditions (Sh = 2) as a function of polymer particle size for low ($R_{ob}$ = 400 g-g-cat-h) and high ($R_{ob}$ = 4000 g-g-cat-h) activity catalysts.

monomer present in the gas phase, a diffusive mechanism for boundary layer mass transfer does not apply. Transport would be due to a total pressure gradient. However, in the case of copolymerization or when the concentration of inerts or hydrogen is significant (as in many industrial gas-phase processes), the diffusive mechanism for external film mass transfer is relevant. Here we perform our analysis using the self-diffusion coefficients for the gases. These should give conservative estimates for the mass transfer resistance in the presence of $H_2$ because the diffusion coefficients for the monomers in $H_2$ are higher.

Figure 14 shows Sh versus Re for gas-phase ethylene and propylene polymerization. Note that the Sherwood number predicted by the Richardson-Szekely correlation drops sharply with decreasing Reynolds number, to values below 2. However, these authors[20] suggest that this drop could be the result of gas back-mixing in their fluidized bed.

Figure 15 shows the mass transfer coefficients estimated by these two correlations as a function of polymer particle size. Because the Ranz-Marshall correlation yields more conservative values for $k_s$ in the range of interest here, we shall use it in the calculations below.

Figure 16 shows the effect of catalyst particle size in gas-phase propylene polymerization on the external film mass transfer driving force for both high- and low-activity catalyst. The maximum $\Delta M$ value for a 100 $\mu$m catalyst particle of high activity is about 0.07 mol/L compared with the bulk concentration in industrial processes of ~1 mol/L. Figure 17 illustrates $\Delta M$ versus $d_p$ for gas-phase ethylene polymerization. As in the case of propylene polymerization, the value of $\Delta M$ is negligible compared with the bulk-phase concentration.

## PARTICLE-FLUID TRANSFER AT LOW REYNOLDS NUMBERS

As indicated above, the lowest values of external film mass transport coefficients in olefin polymerization arise for small particles (i.e., at low Re). Thus, one should analyze heat and mass transfer in this region more closely.

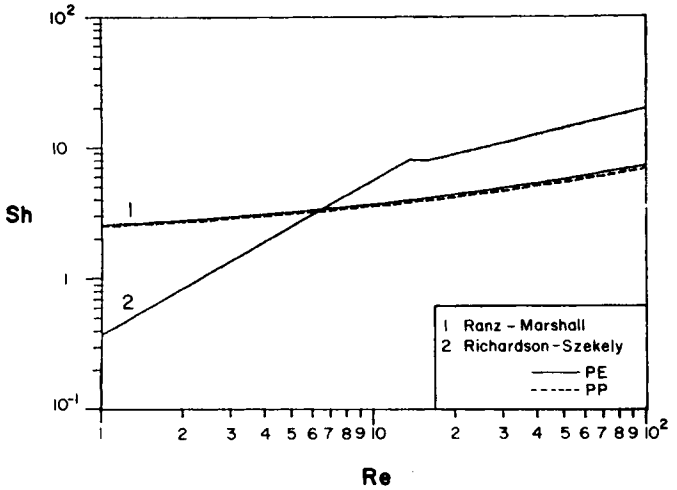


Fig. 14. Comparison of Ranz-Marshall and Richardson-Szekely correlations for the Sherwood number for gas-phase polymerization of ethylene and propylene.

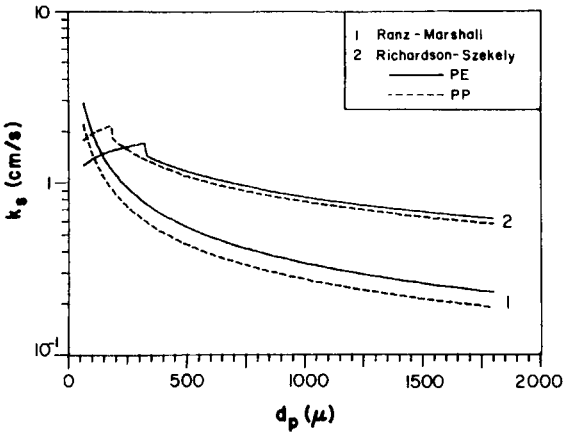


Fig. 15. Mass transfer coefficients for gas-phase polymerization of ethylene and propylene using the Ranz-Marshall and Richardson-Szekely correlations calculated for stirred bed conditions ($u$ = 2 cm/s).

Over the years, there has been considerable disagreement as to the magnitude of Nu and Sh for particle-fluid heat or mass transfer in packed, fluidized and slurry reactors at low Reynolds numbers. The basis of this disagreement is data for packed beds, wire mesh, stirred tanks, and fluidized beds that indicate Nu or Sh as much as several orders of magnitude below the theoretical single-sphere asymptote of 2.[11,15,16,18,20-23] Many workers have offered explanations for these anomalies, mainly in terms of inadequacies of interpretation of the experimental results. The explanations that have been offered are

1. Errors in estimation of the concentration or temperature driving force
2. Axial dispersion of heat and mass
3. Flow maldistribution (channeling and bubbling)
4. Particle interaction effects

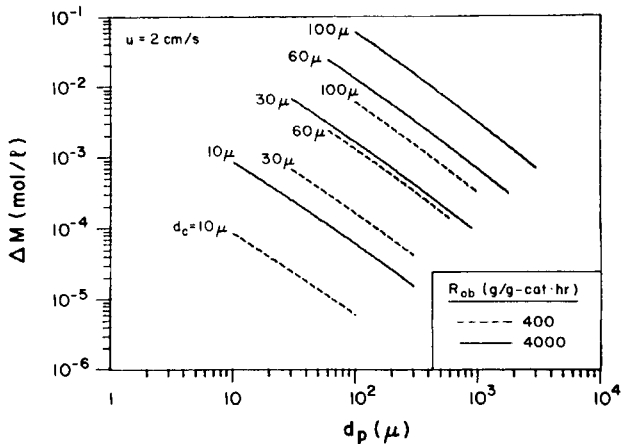


Fig. 16. External film mass transfer resistance in propylene gas-phase polymerization (stirred bed conditions, $u$ = 2 cm/s) as a function of polymer particle size using the Ranz-Marshall correlation. Low ($R_{ob}$ = 400 g-g-cat-h) and high ($R_{ob}$ = 4000 g-g-cat-h) activity catalysts with various catalyst particle sizes.

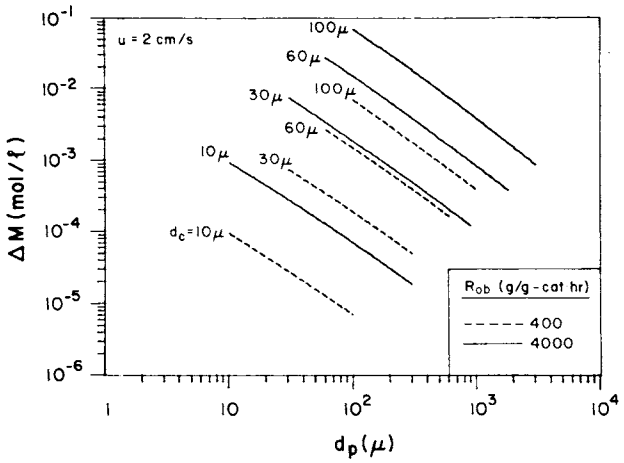


Fig. 17. External film mass transfer resistance in ethylene gas-phase polymerization (stirred bed conditions, $u$ = 2 cm/s) as a function of polymer particle size using the Ranz-Marshall correlation. Low ($R_{ob}$ = 400 g-g-cat-h) and high ($R_{ob}$ = 4000 g-g-cat-h) activity catalysts with various catalyst particle sizes.

The first three explanations suggest that although low apparent values of Nu or Sh are calculated from the data, the actual values for the particle are much higher (i.e., ~2). However, the fourth factor, particle-particle interactions, implies that the actual values of Nu or Sh might be much lower than predicted by classic theory. In the following, we shall present our evaluation of the arguments in this controversy. For a detailed discussion, see Ref. 2A.

Regarding the first factor, it is clear that the problems are due to the necessity for many indirect measurements. Thus, early attainment of equilibrium, averaging over a bed which is not uniform, uncertainties in surface concentrations or temperatures, and other factors, can lead to incorrect values of Nu or Sh. These problems are especially severe at low Reynolds numbers where particles are small and convection effects are of a comparable scale to these uncontrolled factors. Some specific cases are discussed in Refs. 14–16, 18, and 23–25.

Axial dispersion effects at low Reynolds numbers have been extensively discussed by Wakao et al. and others[21,23,24,26–40] for packed beds and by Richardson and Szekely[20] for fluidized beds. It seems clear (especially for packed beds) that axial dispersion effects can explain at least part of the low Nu or Sh anomalies.

The third factor, flow channeling, seems to be a serious effect in both packed beds and fluidized beds. For packed beds Kunii and Suzuki[41] and Martin[42] present a compelling case for the attribution of low values of Nu and Sh to flow channeling. Similarly, Kunii and Levenspiel[11] are convincing in their explanation of fluidized bed data due to bypass of fluid in bubbles.

The fourth factor, involving particle-particle interactions, suggests that for highly concentrated (small void fraction) particulate systems, the single-sphere asymptote, Sh, Nu → 2 is no longer valid. Nelson and Galloway[9] propose that the anomalies in packed or fluidized beds are due to the breakdown of the single-sphere model for low void fractions. They develop a theory

in which the zero flux boundary condition is at a finite distance from the particle surface, dependent on void fraction. Using void fraction as a parameter, they are able to fit observed low Reynolds number data. Rowe[15] extended this correlation to fit liquid fluidized bed data. Tournie et al.[14,43] criticize both of these results on the basis that they are only strictly valid at the no-flow limit and are inconsistent at moderate values of Re. Experimentally, anomalies have been observed for very small particles.[16,18,34,43] This has prompted two other particle-particle interaction explanations:(1) Agglomeration during experimentation so that the particle surface area was in error,[34] and (2) the suggestion that very small particles are swept along in small eddies with essentially zero relative velocity and these eddies have abnormal concentration and temperature fields due to lack of mixing on this small scale.[16]

To summarize, it seems clear that the observed anomalies in Sh and Nu at low Re in *packed* or *fluidized* beds can be adequately explained in terms of experimental artifact, axial dispersion effects, and flow bypassing or channeling. Furthermore, the present weight of opinion in the literature seems to support these explanations. However, for slurry reactors, only experimental artifacts, such as particle agglomeration or particle-particle interactions, would seem to explain the two data points of Nagata and Nishikawa[16] showing anomalies at very small particle size.

In conclusion, it appears that the so-called anomalous data for Sh and Nu at low Re can be explained by inadequacies of experimental interpretation that cause the true rates of particle-particle mass and heat transfer to be masked by other effects. Further studies of highly concentrated liquid-solid systems, particularly with small particles, would be justified in order to resolve the remaining questions in this special situation. However, for the present, it seems that for predicting single particle mass and heat transfer, correlations that show a stagnation asymptote of $\sim 2$ are the most acceptable.

## HEAT TRANSFER IN THE PARTICLE BOUNDARY LAYER

It was shown in Part III[1] that temperature gradients within the microparticle as well as within the macroparticle will normally be negligible. Thus if the growing polymer particle is to have a temperature higher than the surrounding fluid, it must be due to significant heat transfer resistance across the external boundary layer. In this section we investigate that possibility.

As in the case of mass transfer in the external boundary layer, we may establish a quasi-steady-state energy balance

$$h A_p \Delta T = \frac{\rho_c V_c R_{ob} (-\Delta H_p)}{MW} \tag{12}$$

where $h$ is the external film heat transfer coefficient and $(-\Delta H_p)$ is the heat of reaction. Thus the temperature rise across the external boundary layer is predicted from

$$\Delta T = \frac{\rho_c R_c^3 R_{ob}(-\Delta H_p)}{3hR_p^2 \mathrm{MW}} \tag{13}$$

As in the case of mass transfer, correlations must be used to determine the external film heat transfer coefficient $h$.

Correlations for particle-fluid heat transfer that have been proposed are as follows:

1. Ranz-Marshall correlation[5] for a single sphere in a fluid medium moving with relative velocity $u$:

$$\mathrm{Nu} = 2 + 0.6\mathrm{Re}^{1/2}\mathrm{Pr}^{1/3} \tag{14}$$

where

$$\mathrm{Nu} = \frac{hd_p}{k_f}$$

$$\mathrm{Re} = \frac{\rho u d_p}{\mu}$$

$$\mathrm{Pr} = \frac{\mu C_{pf}}{k_f}$$

2. Kunii and Levenspiel[11] correlation for fluidized beds*:

$$\mathrm{Nu} = 0.03\mathrm{Re}^{1.3} \tag{15}$$

3. Kettenring et al.[44] correlation for fluidized beds:

$$\mathrm{Nu} = 0.0135\mathrm{Re}^{1.3} \tag{16}$$

4. Zenz and Othmer[45] correlation for fluidized beds:

$$\mathrm{Nu} = 0.017\mathrm{Re}^{1.21} \tag{17}$$

5. Borodulya et al.[46] correlation for fluidized beds:

$$\mathrm{Nu} = 0.37\mathrm{Re}^{0.71}\mathrm{Pr}^{0.31} \tag{18}$$

6. Nelson and Galloway[9] correlation for concentrated particle-fluid systems with fluid fraction $\epsilon$:

$$\mathrm{Nu} = \frac{2\zeta + \left[\dfrac{2\zeta^2(1-\epsilon)^{1/3}}{[1-(1-\epsilon)^{1/3}]^2} - 2\right]\tanh\,\zeta}{\left[\dfrac{\zeta}{1-(1-\epsilon)^{1/3}} - \tanh\,\zeta\right]} \tag{19}$$

* The coefficient in this equation is given incorrectly in Ref. 11.

where

$$\zeta = [(1 - \epsilon)^{-1/3} - 1]\frac{\alpha}{2}\mathrm{Re}^{1/2}\mathrm{Pr}^{1/3}$$

The predicted values of Nu versus Re for the various correlations are plotted in Fig. 18 for gas-phase propylene polymerization. Note that the Ranz-Marshall correlation predicts the highest values of Nu and most of the fluidized bed correlations predict very similar values. Predictions from the Nelson and Galloway correlation depend on the value of the fluid fraction $\epsilon$. Here $\epsilon = 0.7$ was chosen as representative of industrial conditions in both liquid- and gas-phase polymerization in continuous reactors. As $\epsilon \rightarrow 1$, the Nelson and Galloway predictions approach those of Ranz and Marshall.

## Liquid Slurry Polymerization

In liquid slurry polymerization, the slurry is agitated vigorously to ensure suspension of the solids and also to facilitate absorption of monomer (when monomer is fed as a gas to the reactor) and chain transfer agents. As in the case of the mass transfer coefficients discussed earlier, the heat transfer coefficients may be larger than those estimated using the terminal velocity of the particles. On the other hand, it has been suggested[9,41,42] that the Ranz-Marshall correlation seriously overestimates the Nusselt number at low Re, but as indicated in the last section, there is some uncertainty about the accuracy of the correlations that predict Nu < 2 at low Reynolds numbers. Thus more definitive research is required to confirm the actual heat transfer coefficients for very small particles. Thus, to be conservative, we shall compare predictions from the Ranz-Marshall correlation with that proposed by Nelson and Galloway to account for high particle concentrations. Figure 19 shows the ratio of Nusselt numbers (heat transfer coefficients) predicted by the Nelson-Galloway correlation and the Ranz-Marshall correlation for propylene slurry polymerization. From this figure, it is evident that for large fluid fractions (low solids concentration), the two correlations predict essentially identical values, but at high solids concentrations, considerable deviations may be expected. Figures 20 and 21 show the actual heat transfer coefficients predicted by the Ranz-Marshall

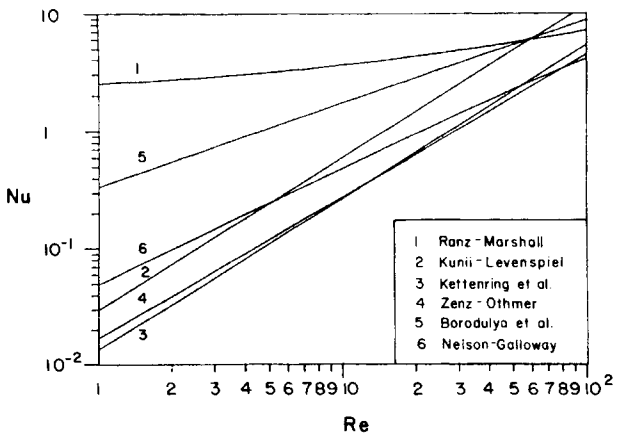


Fig. 18. Comparison of correlations for the Nusselt number for external film heat transfer in propylene gas-phase polymerization.

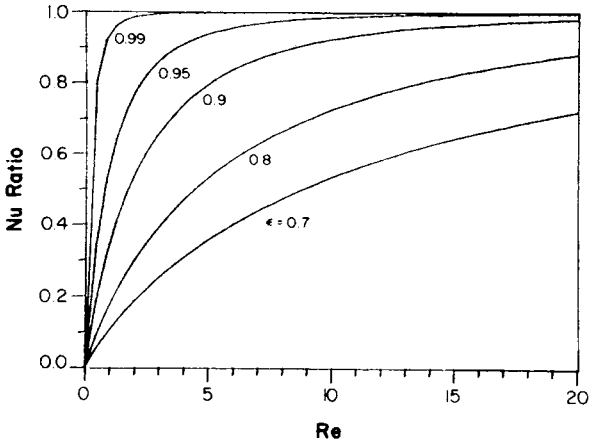


Fig. 19. Ratio of Nusselt numbers calculated by the Ranz-Marshall and Nelson-Galloway correlations for propylene slurry polymerization ($\epsilon$ is volume fraction fluid).

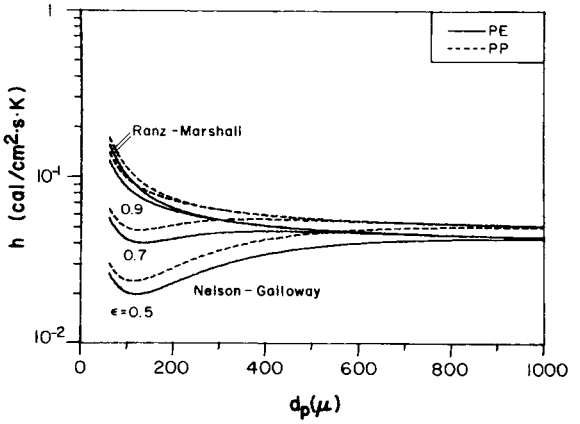


Fig. 20. Heat transfer coefficients for slurry polymerization of ethylene and propylene calculated by the Ranz-Marshall correlation and Nelson-Galloway correlation for various values of $\epsilon$. Initial catalyst particle size $d_c = 60$ $\mu$m.

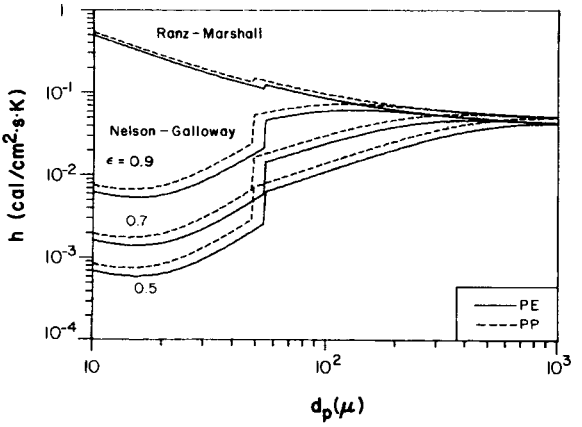


Fig. 21. Heat transfer coefficients for slurry polymerization of ethylene and propylene calculated by the Ranz-Marshall correlation and Nelson-Galloway correlation for various values of $\epsilon$. Initial catalyst particle size $d_c = 10$ $\mu$m.

and the Nelson-Galloway correlations at several fluid fractions. The figures show that the difference in the predicted heat transfer coefficients can be an order of magnitude or more for very small particles in high concentration. For semibatch polymerizations commonly conducted in the laboratory, the solids concentration at the beginning of polymerization when the particles are small would be rather low: thus under these conditions, the difference between the correlations would not be very significant. However, for continuous polymerization under industrial conditions (solids loadings of 30–50%), the Nelson-Galloway predictions would deviate significantly from those of the Ranz-Marshall correlation. As an illustration, Fig. 22 shows the predictions of the Ranz-Marshall correlation for propylene slurry polymerization using low- and high-activity catalyst. From this figure, one sees that significant temperature rises for low-activity catalyst can be expected only for catalyst particles over 100 $\mu$m. However, for high-activity catalyst, particles larger than ~20 $\mu$m will show significant overheating. In particular, for the largest particle of high-activity catalyst, the particles would have to grow to several times their initial diameter for the temperature rise to become insignificant. Hence, the external film temperature resistance might be important for a noticeable period of time. The Nelson-Galloway correlation, as shown in Fig. 23, predicts even higher temperature rises, in some cases even exceeding the softening point of the polymer. This would result in polymer particle fusing or agglomeration for slurry polymerization. Note that although the Ranz-Marshall correlation indicates that smaller catalyst particles lessen the overheating problem, the Nelson-Galloway correlation predicts the worst overheating with the very smallest catalyst particles. Figures 24 and 25 illustrate the predictions of the two correlations for the polymerization of ethylene. The temperature rises predicted for ethylene polymerization are somewhat higher than those for propylene. The Ranz-Marshall correlation shows moderate overheating for high-activity catalyst, but the Nelson-Galloway correlation predicts a

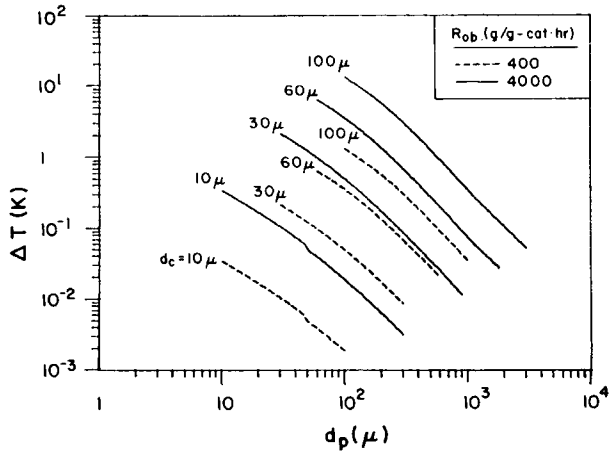


Fig. 22. External film heat transfer resistance in propylene slurry polymerization as a function of polymer particle size using the Ranz-Marshall correlation for low ($R_{ob}$ = 400 g-g-cat-h) and high ($R_{ob}$ = 4000 g-g-cat-h) activity catalysts with various catalyst particle sizes.

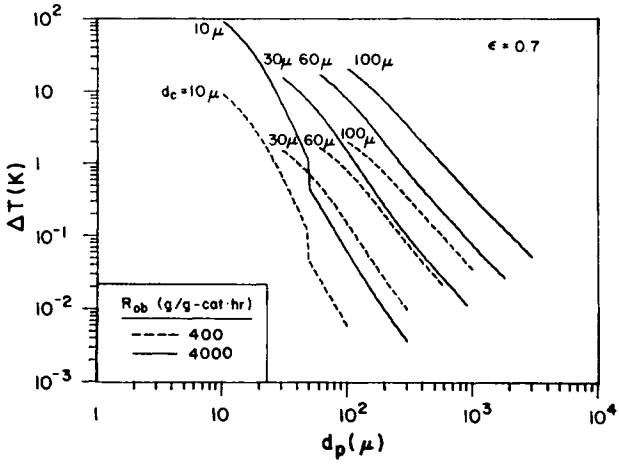


Fig. 23. External film heat transfer resistance in propylene slurry polymerization as a function of particle size using the Nelson-Galloway correlation ($\epsilon = 0.7$). Low ($R_{ob} = 400$ g-g-cat-h) and high ($R_{ob} = 4000$ g-g-cat-h) activity catalysts with various catalyst particle sizes.

significant $\Delta T$ even for low-activity catalyst, and for high-activity catalyst the initial temperature rise would be over 30 K for all particle sizes.

The analysis of this section would suggest that, for slurry polymerization with high-cativity catalysts, serious particle overheating could occur immediately after catalyst injection—especially in reactors with high solids concentration. This would suggest that one may wish to delay achievement of full activity of the catalyst until this initial "hot" phase in the particle lifetime is over. Fortunately, this initial overheating is mitigated somewhat by both intraparticle and boundary layer mass transfer resistance early in the particle lifetime, as has been discussed. Because heat and mass transfer resistance are at their peak together, the local rate of polymerization will

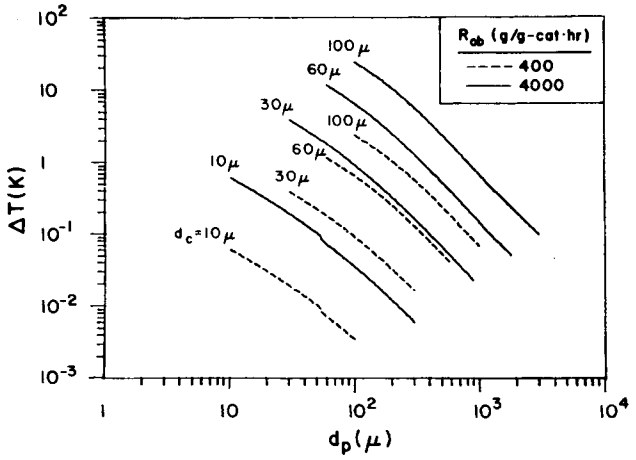


Fig. 24. External film heat transfer resistance in ethylene slurry polymerization as a function of polymer particle size using the Ranz-Marshall correlation for low ($R_{ob} = 400$ g-g-cat-h) and high ($R_{ob} = 4000$ g-g-cat-h) activity catalysts with various catalyst particle sizes.

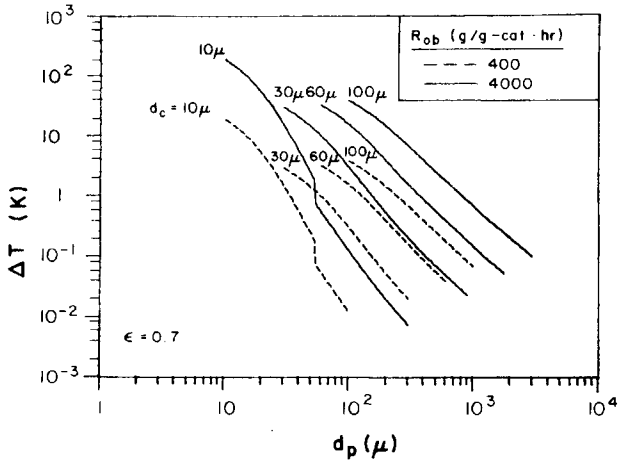


Fig. 25. External film heat transfer resistance in ethylene slurry polymerization as a function of particle size using the Nelson-Galloway correlation ($\epsilon = 0.7$). Low ($R_{ob}$ = 400 g-g-cat-h) and high ($R_{ob}$ = 4000 g-g-cat-h) activity catalysts with various catalyst particle sizes.

be reduced by mass transfer just when particle overheating might be a problem. These combined effects will be illustrated below through model simulation.

## Gas-Phase Polymerization

As mentioned previously and illustrated in Fig. 18, there is considerable lack of agreement among the values of the Nusselt number predicted by the correlations given in eqs. (14) through (19). Although the Ranz-Marshall correlation appears preferable to use, we shall also include as a "worst case" predictions using "apparent" Nusselt numbers from the Kunii-Levenspiel correlation, although this is thought to greatly underestimate $h$ at low Reynolds numbers. Calculations have been made using a relative velocity of 2 cm/s, which would be appropriate for stirred bed reactors,[19] and 20 cm/s, corresponding to some regions in a fluidized bed.[11] The predicted temperature rise for propylene polymerization under stirred bed conditions using the Ranz-Marshall correlation is illustrated in Fig. 26; Fig. 27 shows the $\Delta T$ for polymerization in parts of a fluidized bed. As evident from these figures, significant temperature rises may be anticipated for low-activity catalyst ($R_{ob}$ = 400 g/g-cat/h), and the temperature rise for high-activity catalyst may be sufficient to cause polymer softening, sticking, and agglomeration problems. For large particles of high-activity catalyst, a significant temperature rise of a few degrees Kelvin should persist throughout polymerization. Figures 28 and 29 show the calculated temperature rise for propylene polymerization using the Kunii-Levenspiel correlation for the respective conditions. Note that the Kunii-Levenspiel correlation is much more sensitive to Re, that is, to the relative velocity. For stirred bed conditions, the correlation predicts large temperature rises even for low-activity catalyst, and for high-activity catalyst, the melting point of the polymer would be reached for every catalyst size. Under high-velocity fluidized bed conditions, the temperature rise would be much smaller for low-activity

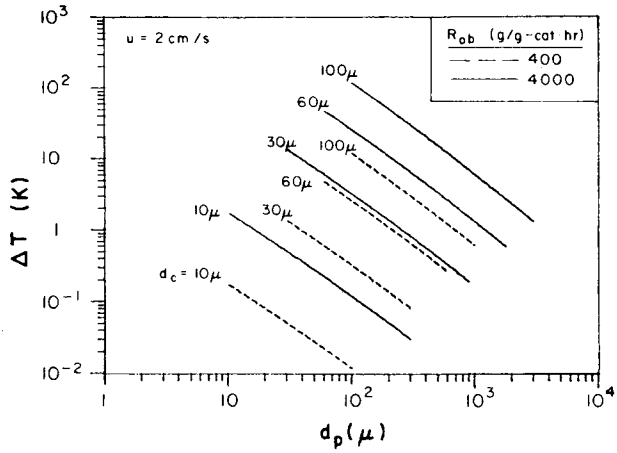


Fig. 26. External film heat transfer resistance in propylene gas-phase polymerization (stirred bed conditions, $u$ = 2 cm/s) as a function of polymer particle size using the Ranz-Marshall correlation. Low ($R_{ob}$ = 400 g-g-cat-h) and high ($R_{ob}$ = 4000 g-g-cat-h) activity catalysts with various catalyst particle sizes.

catalyst but would be greater than 10 K for high-activity catalyst at all catalyst sizes. Because of the Reynolds number dependence, the falloff in $\Delta T$ with increasing particle diameter is very sharp for the Kunii-Levenspiel correlation.

For ethylene polymerization, the Ranz-Marshall correlation predictions are illustrated in Figs. 30 and 31 for stirred and fluidized bed conditions, respectively. The predicted values of $\Delta T$ lie a few degrees Kelvin above the values predicted for propylene polymerization. The predictions for the Kunii-Levenspiel correlation for ethylene polymerization are not shown but also indicate significant overheating of the polymer particles.

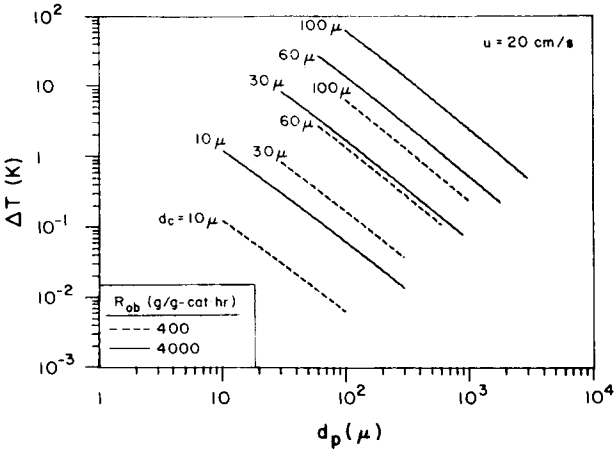


Fig. 27. External film heat transfer resistance in propylene gas-phase polymerization (fluidized bed conditions, $u$ = 20 cm/s) as a function of particle size using the Ranz-Marshall correlation for low ($R_{ob}$ = 400 g-g-cat-h) and high ($R_{ob}$ = 4000 g-g-cat-h) activity catalysts with various catalyst particle sizes.

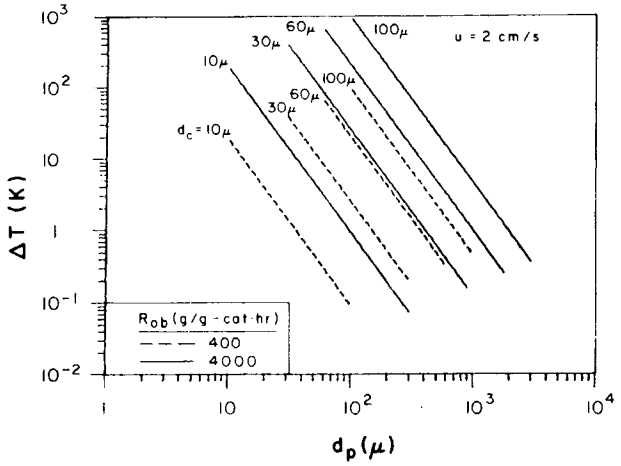


Fig. 28. External film heat transfer resistance in propylene gas-phase polymerization (stirred bed conditions, $u$ = 2 cm/s) as a function of polymer particle size using the Kunii-Levenspiel correlation. Low ($R_{ob}$ = 400 g-g-cat-h) and high ($R_{ob}$ = 4000 g-g-cat-h) activity catalysts with various catalyst particle sizes.

From the results here, it seems clear that the Kunii-Levenspiel correlation is not appropriate for olefin polymerization at low Reynolds numbers. If it were, none of the stirred bed gas-phase olefin polymerization processes in operation today could exist because the predicted particle temperatures are above the softening point of the polymer. Thus we shall interpret the results in terms of the Ranz-Marshall correlation.

As indicated in Figs. 26, 27, 30, and 31, operating a gas-phase reactor with either low- or high-activity catalyst would lead to a significant particle temperature rise that would influence observed kinetics early in the poly-

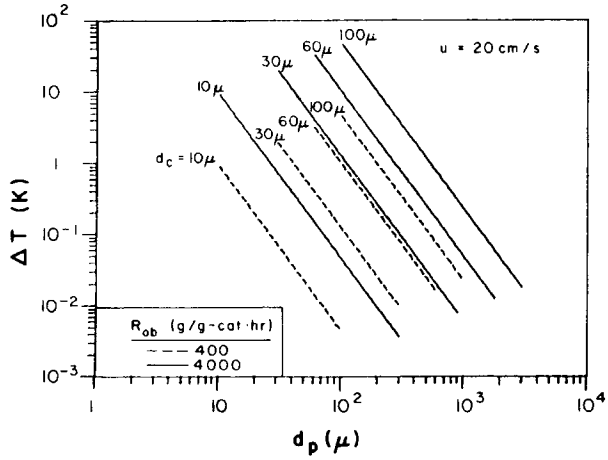


Fig. 29. External film heat transfer in propylene gas-phase polymerization (fluidized bed conditions, $u$ = 20 cm/s) as a function of particle size using the Kunii-Levenspiel correlation for low ($R_{ob}$ = 400 g-g-cat-h) and high ($R_{ob}$ = 4000 g-g-cat-h) activity catalysts with various catalyst particle sizes.

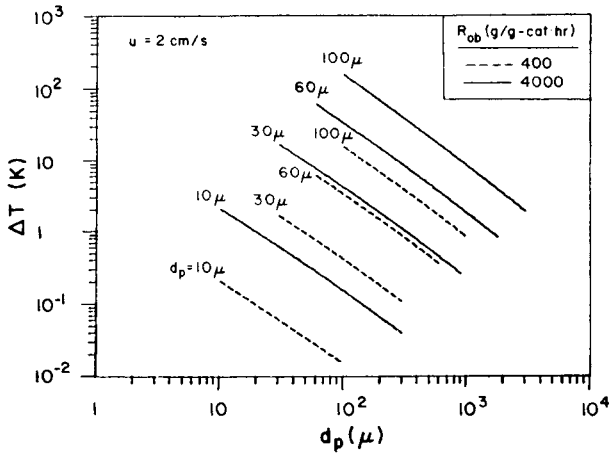


Fig. 30. External film heat transfer resistance in ethylene gas-phase polymerization (stirred bed conditions, $u$ = 2 cm/s) as a function of polymer particle size using the Ranz-Marshall correlation. Low ($R_{ob}$ = 400 g-g-cat-h) and high ($R_{ob}$ = 4000 g-g-cat-h) activity catalysts with various catalyst particle sizes.

merization and could lead to agglomeration and sticking of polymer particles for high-activity catalyst above 30–60 μm in diameter. This is consistent with what has been observed under certain conditions in both stirred bed and fluidized bed industrial reactors.

## PARTICLE SIMULATIONS

In this section, we will present some simulations of catalyst particles in olefin polymerization to illustrate the phenomena that may be expected. The simulations are based on the multigrain model described in Part III[1] with the parameters given in Table I. Further details of this model and

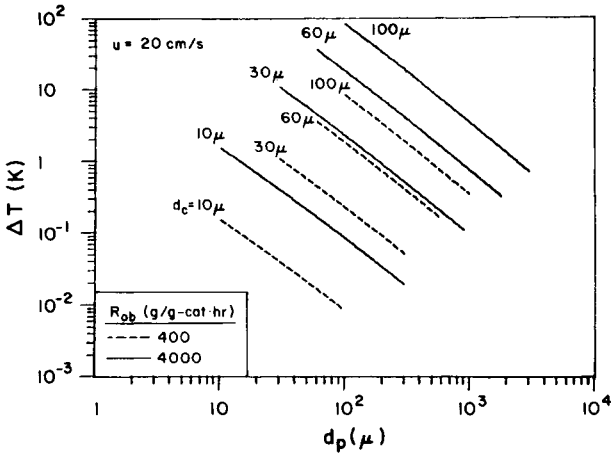


Fig. 31. External film heat transfer resistance in ethylene gas-phase polymerization (fluidized bed conditions, $u$ = 20 cm/s) as a function of particle size using the Ranz-Marshall correlation for low ($R_{obh}$ = 400 g-g-cat-h) and high ($R_{ob}$) = 4000 g-g-cat-h) activity catalysts with various catalyst particle sizes.

TABLE 1
Parameters and Average Activities for Particle Simulations

| Figure | Polymerization | Curve | Intrinsic activity (g/g-cat.h) | Average activity[a] (g/g-cat.h) | Comments[b] |
|---|---|---|---|---|---|
| 32 | Ethylene gas | $\tau_c = 0$ | 4000 | —[c] | |
| | | $\tau_c = 0.5$ s | 4000 | 4820 | |
| | | $\tau_c = 1$ s | 4000 | 3790 | |
| | | $\tau_c = 5$ s | 4000 | 1180 | |
| 33 | Ethylene gas | $d_c = 10$ μm | 4000 | 3440 | |
| | | $d_c = 30$ μm | 4000 | 4820 | |
| | | $d_c = 60$ μm | 4000 | —[c] | |
| 34 | Ethylene gas | $\tau_c = 0$ | 400 | 492 | |
| | | $\tau_c = 0.5$ s | 400 | 420 | |
| | | $\tau_c = 5$ s | 400 | 108 | |
| 35 | Ethylene | Slurry | 4000 | 2460 | For slurry case, |
| | | Gas, $u = 2$ cm/s | 4000 | 4820 | $D_l = 10^{-5}$ cm²/s |
| | | Gas, $u = 20$ cm/s | 4000 | 4600 | |
| 36 | Propylene | Slurry | 4000 | 3050 | For slurry case, |
| | | Gas, $u = 2$ cm/s | 4000 | 4380 | $D_l = 10^{-5}$ cm²/s |
| | | Gas, $u = 20$ cm/s | 4000 | 3820 | |
| 37 | Ethylene gas | $d_c = 30$ μm | 4000 | 3980 | |
| | | $d_c = 60$ μm | 4000 | 4210 | |
| 38 | Ethylene slurry | $d_c = 30$μm | 8000 | 2480 | $r_c = 0.01$ μm |
| | | $d_c = 60$ μm | 8000 | 360 | |
| | | $d_c = 100$ μm | 8000 | 240 | |
| 39 | Ethylene slurry | $d_c = 30$ μm | 8000 | 7010 | $r_c = 0.01$ μm |
| | | $d_c = 60$ μm | 8000 | 3250 | $D_l = 5 \times 10^{-6}$ cm²/s |
| | | $d_c = 100$ μm | 8000 | 830 | |
| 40 | Ethylene slurry | $d_c = 30$ μm | 8000 | 7590 | $r_c = 0.01$ μm |
| | | $d_c = 60$ μm | 8000 | 5720 | $D_l = 10^{-5}$ cm²/s |
| | | $d_c = 100$ μm | 8000 | 2120 | |
| 41 | Ethylene gas | Ranz-Marshall | 4000 | 3980 | |
| | | Kunii-Levenspiel | 4000 | 4220 | |
| 42,43 | Ethylene slurry | Ranz-Marshall | 4000 | 2460, 3800 | $r_c = 0.01$ μm |
| | | Nelson-Galloway | 4000 | 2860, 3810 | $D_l = 10^{-5}$ cm²/s |

[a] Yield at end of simulation divided by simulation time shown.

[b] Unless otherwise stated, the following parameters were used. Ethylene gas: $r_c = 0.1$ μm, $D_l = \infty$ (no macroparticle diffusion resistance, $D_s = 10^{-7}$ cm²/s, $M_b = 1$ mol/L. Propylene gas: same as ethylene gas. Ethylene slurry: $r_c = 0.1$ μm, $D_l = 10^{-6}$ cm²/s, $D_s = 10^{-7}$ cm²/s, $M_b = 2$ mol/L. Propylene slurry: same as ethylene slurry except $M_b = 4$ mol/L.

[c] Melting point of polymer reached.

its predictions will be presented in a future paper. Although the simulations include the effects of intraparticle gradients, we shall primarily discuss the predictions of external film resistance. Unless otherwise stated, the Ranz-Marshall correlation was used in the simulations. The intrinsic catalyst activity (i.e., rate at bulk conditions) is indicated in Table I together with the actual observed average rate.

As mentioned previously, for gas-phase polymerization the permeation of the catalyst particle by monomer and its consequent breakup is expected to be quite short, of the order of seconds at most. However, the exact time

scale will depend on such factors as catalyst activity, monomer concentration, temperature, and catalyst pore structure. Thus we shall choose several reasonable time scales and compare the simulation results. Figure 32 shows simulations of the heat and mass transfer resistances for a high-activity catalyst (intrinsic activity, 4000 g-g-cat-h) in ethylene gas-phase polymerization under stirred bed conditions using the Ranz-Marshall correlation for both resistances. The uppermost curve is for "instantaneous" breakup; the lower curves are for cases in which the catalyst sites are "activated" in an exponential fashion with time constants of 0.5, 1, and 5 s. As this figure shows, instantaneous breakup results in a temperature rise up to the melting point of the polymer (assumed to be an upper bound), but significantly, any delay in the catalyst reaching its full activity can mitigate the large $\Delta T$ to a considerable extent. This has the interesting implication that the problems caused by particle overheating (such as sticking) can be at least partially avoided by activating the catalyst in situ. Also of importance is the effect of catalyst particle size, as suggested by earlier figures. Figure 33 shows the effect of particle size for 0.5-s catalyst "activation" in ethylene gas-phase polymerization under stirred bed conditions. The temperature rise is insignificant for the 10-$\mu$m catalyst particles and fairly significant for the 30-$\mu$m particles, but the temperature is predicted to reach the melting point of the polymer with 60-$\mu$m catalyst particles. For low-activity catalyst ($R_{ob} \sim 400$ g-g-cat-hr), the temperature rise for 60-$\mu$m catalyst particles is shown in Fig. 34. In this case, a maximum $\Delta T$ of around 6 K is predicted, even for the worst case of instantaneous breakup.

Figure 35 compares the behavior of the resistances with time for ethylene polymerization under three conditions: slurry, gas-phase stirred bed, and high-velocity gas-phase fluidized bed. In this figure, the catalyst was assumed to be activated with a characteristic time of 0.5 s. As can be seen

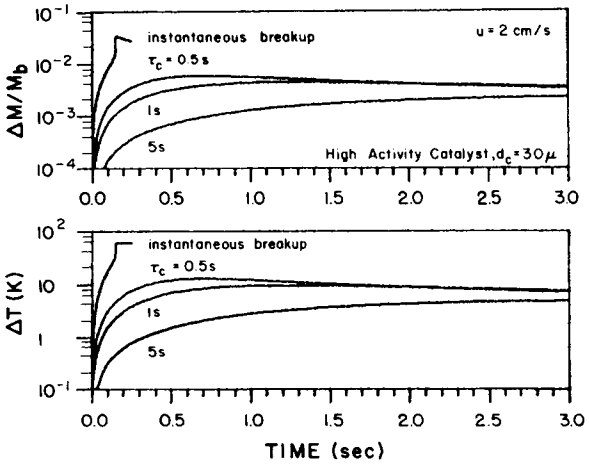


Fig. 32. External film heat and mass transfer resistances in gas-phase polymerization of ethylene under stirred bed conditions ($u$ = 2 cm/s) with high-activity catalyst. Effect of characteristic breakup time of catalyst $\tau_c$. The Ranz-Marshall correlation was employed. Average rates (g-g-cat-h): $\tau_c$ = 0.5 s, 4820; $\tau_c$ = 1 s, 3790; $\tau_c$ = 5 s, 1180.

TABLE II
Summary of Conclusions with Respect to Heat and Mass Transfer Resistances

| Reaction Medium | Microparticle gradients | | Macroparticle gradients | | External film gradients | |
|---|---|---|---|---|---|---|
| | Thermal | Concentration | Thermal | Concentration | Thermal | Concentration |
| Gas | Negligible | Can be significant for high-activity catalysts and for those yielding large primary crystallites after breakup | Negligible except for large particles of high-activity catalyst early in particle lifetime | Negligible except for large particles of high-activity catalyst early in particle lifetime | Often very significant during initial stages of particle growth | Negligible |
| Liquid slurry | Negligible | Can be significant for high-activity catalysts and for those yielding large primary crystallites after breakup | Negligible | Usually significant, especially early in particle lifetime | Negligible except for large high-activity catalyst particles early in particle growth | Negligible except for large high-activity catalyst particles early in particle growth |

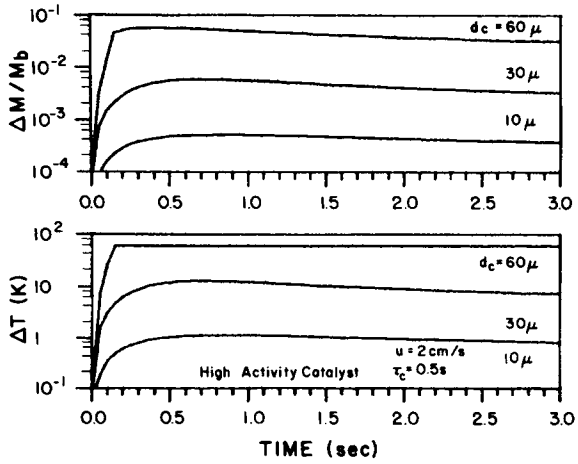


Fig. 33. External film heat and mass transfer resistances in gas-phase polymerization of ethylene under stirred bed conditions ($u$ = 2 cm/s) with high-activity catalyst. Effect of catalyst particle size. Characteristic breakup time $\tau_c$ = 0.5 s. The Ranz-Marshall correlation was employed. Average rates (g-g-cat-h); $d_c$ = 10 μm, 3440; $d_c$ = 30 μm, 4820.

here, the mass transfer resistance is greatest (but still insignificant) for slurry polymerization. In gas-phase polymerization with high-activity catalyst, the temperature resistance is significant during the early stages of polymerization, albeit not as high as in the case when full catalyst site activity is assumed at $t$ = 0. The temperature rise for high gas velocity fluidized bed conditions is roughly half that for stirred bed conditions. Figure 36 shows the situation for propylene polymerization with a high-activity catalyst. Clearly, the qualitative trends are similar. For both these figures, the "observed" rate for the slurry case is a 3-s average and is lower than the ultimate rate, which is close to the intrinsic rate of 4000. This is due

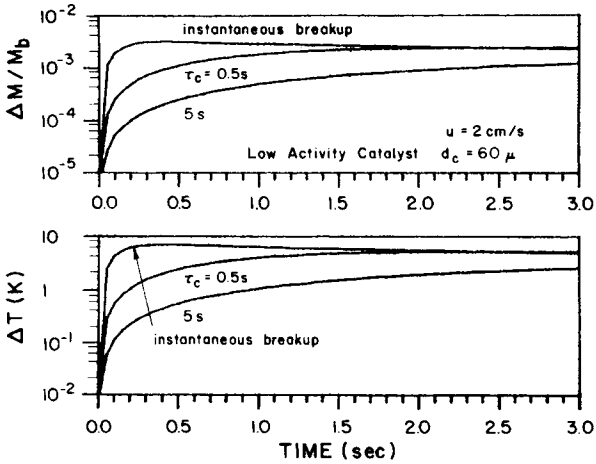


Fig. 34. External film heat and mass transfer resistances in gas-phase polymerization of ethylene under stirred bed conditions ($u$ = 2 cm/s) with low-activity catalyst. Effect of characteristic breakup time of catalyst $\tau_c$. The Ranz-Marshall correlation was employed. Average rates (g-g-cat-h): $\tau_c$ = 0, 492; $\tau_c$ = 0.5 s, 420; $\tau_c$ = 5 s, 108.

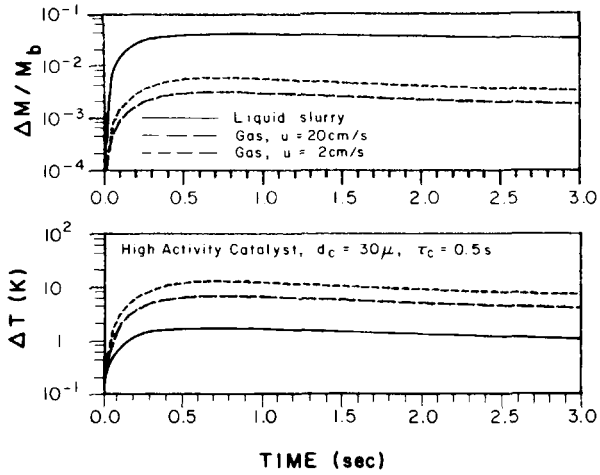


Fig. 35. Effect of polymerization conditions on external film heat and mass transfer resistances in ethylene polymerization over high-activity catalyst with breakup time $\tau_c = 0.5$ s. The Ranz-Marshall correlation was employed: (—) slurry polymerization, average rate, 2460 g-g-cat-h; (— — —) gas fluidized bed ($u = 20$ cm/s), average rate, 4600 g-g-cat-h; (- - -) gas stirred bed ($u = 2$ cm/s), average rate, 4820 g-g-cat-h).

to intraparticle mass transfer resistance in slurry, which is very significant for short times even with $D_l = 10^{-5}$ cm$^2$/s.

It is also instructive to look at these phenomena over a time scale comparable to the residence time of the particles in a reactor. Figure 37 illustrates the trends in the resistances for a residence time of 1 h with 30-μm and 60-μm particles of a high-activity catalyst in ethylene gas-phase polymerization. Figures 38 through 40 illustrate the external film resistances

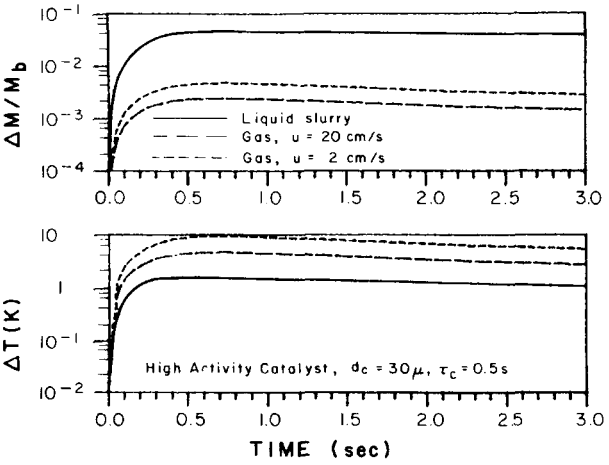


Fig. 36. Effect of polymerization conditions on external film heat and mass transfer resistances in propylene polymerization over high-activity catalyst with breakup time $\tau_c = 0.5$ s. The Ranz-Marshall correlation was employed: (—) slurry polymerization, average rate, 3050 g-g-cat-h; (— — —) gas fluidized bed ($u = 20$ cm/s), average rate, 3820 g-g-cat-h; (- - -) gas stirred bed ($u = 2$ cm/s), average rate, 4380 g-g-cat-h).

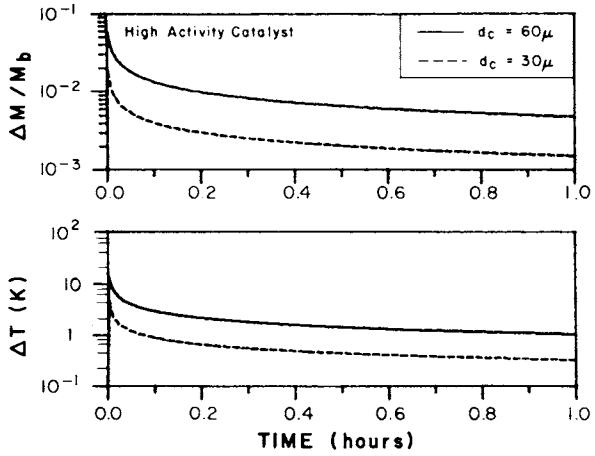


Fig. 37. External film heat and mass transfer resistances in gas-phase polymerization of ethylene under stirred bed conditions ($u$ = 2 cm/s) over high-activity catalyst. Trends over 1 h with catalyst particle size $d_c$ = 30 and 60 μm. The Ranz-Marshall correlation was employed ($\tau_c$ = 0.5 s). Average rates (g-g-cat-h): $d_c$ = 30 μm, 3980; $d_c$ = 60 μm, 4210.

for various particle sizes of very high intrinsic activity (8000 g-g-cat-h) catalyst, with large particle diffusion coefficient $D_l = 10^{-6}$, $5 \times 10^{-6}$ and $10^{-5}$ cm²/s, respectively. A value of $r_c = 0.01\mu$ was chosen for these simulations to be consistent with such high intrinsic activity. In this range of $D_l$, which is considered physically reasonable,[1] the lower values might arise when there is a high soluble polymer content in the slurry or with very low polymer particle porosity. As the simulations show, the time for the external film resistances to remain significant is generally less than a few

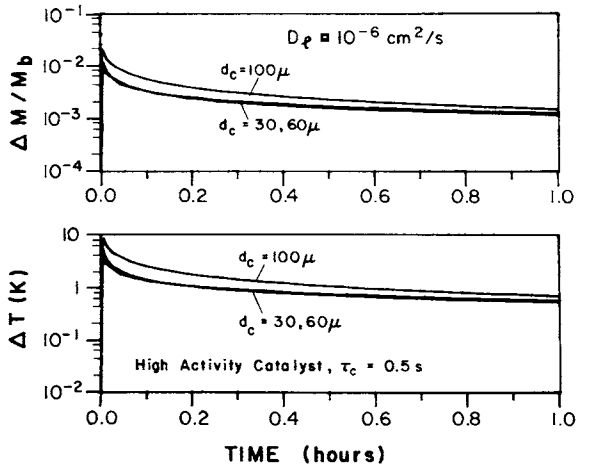


Fig. 38. External film heat and mass transfer resistances in slurry polymerization of ethylene over high-activity catalyst, large particle diffusivity $D_l = 10^{-6}$ cm²/s. Trends over 1 h with catalyst particle size $d_c$ = 30, 60, and 100 μm. The Ranz-Marshall correlation was employed ($\tau_c$ = 0.5 s). Average rates (g-g-cat-h): $d_c$ = 30 μm, 2480; $d_c$ = 60 μm, 360; $d_c$ = 100 μm, 240.

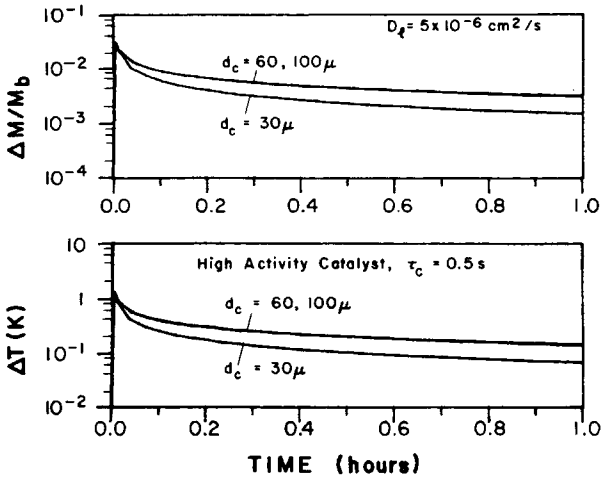


Fig. 39. External film heat and mass transfer resistances in slurry polymerization of ethylene over high-activity catalyst, large particle diffusivity $D_l = 5 \times 10^{-6}$ cm²/s. Trends over 1 h with catalyst particle size $d_c$ = 30, 60, and 100 μm. The Ranz-Marshall correlation was employed ($\tau_c$ = 0.5 s). Average rates (g-g-cat-h): $d_c$ = 30 μm, 7010; $d_c$ = 60 μm, 3250; $d_c$ = 200 μm, 830.

minutes. Note that for a catalyst with intrinsic activity 8000 g-g-cat-h, the actual observed reaction rates would vary dramatically with catalyst particle size. This lowering of the observed rate is due primarily to intraparticle mass transfer resistances at the macroparticle level, as discussed in the previous paper in this series.[1] For the conditions of the simulation, diffusion resistance at the microparticle level would be negligible.

Finally, some simulations were carried out using other Nusselt number correlations for $\Delta T$. At short times, the Kunii-Levenspiel correlation pre-

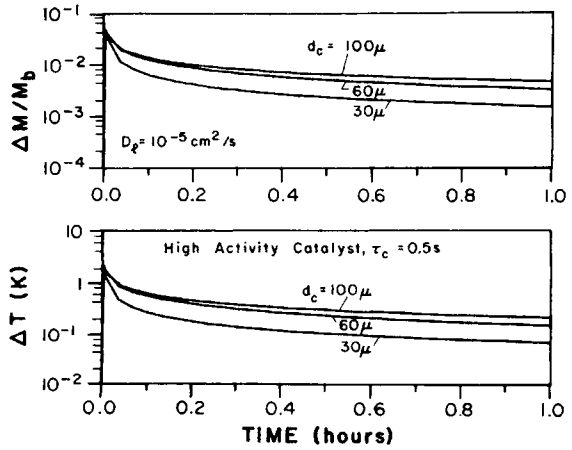


Fig. 40. External film heat and mass transfer resistances in slurry polymerization of ethylene over high-activity catalyst, large particle diffusivity $D_l = 10^{-5}$ cm²/s. Trends over 1 h with catalyst particle size $d_c$ = 30, 60, and 100 μm. The Ranz-Marshall correlation was employed ($\tau_c$ = 0.5 s). Average rates (g-g-cat-h): $d_c$ = 3- μm, 7590; $d_c$ = 60 μm, 5720; $d_c$ = 100 μm, 2120.

dicts a temperature rise to the melting temperature in gas-phase polymerization, even for low-activity catalysts with a characteristic time for site activation as long as 5 s. However, on a longer time scale, Fig. 41 shows that the very large temperature excursions predicted by this correlation last for less than 1 min even though this would suffice to cause the particles to agglomerate. As indicated by Fig. 41, the Kunii-Levenspiel correlation predicts a particle temperature rise considerably higher than does the Ranz-Marshall correlation. For slurry polymerization, Fig. 42 compares $\Delta T$ predicted by the Ranz-Marshall and Nelson-Galloway correlations at short times. It is seen that a maximum $\Delta T$ of the order of 10 K is predicted by the Nelson-Galloway correlation in this case. Extending the time scale for this case, as shown in Fig. 43, confirms that the particle temperature rise becomes insignificant after 10 min even for the Nelson-Galloway correlation.

## CONCLUSIONS

In slurry polymerizations, calculations based on the Ranz-Marshall correlation suggest the presence of a significant external film mass transfer resistance for high-activity catalysts at the outset of polymerization. This effect would be especially strong for large catalyst particles. However, as soon as the polymer particle grows to 5–10 times the original catalyst size, this resistance becomes insignificant. This growth occurs very rapidly in the case of the high-activity catalysts considered, as the simulations illustrate. In gas-phase polymerization (for mixtures of monomer with comonomer or hydrogen), one would never expect significant mass transfer resistance in the external film even for the most active catalysts. Hence, it seems reasonable to conclude that, in general, external film mass transfer resistances are only a significant factor early in the polymer particle lifetime for slurry polymerization with large, highly active catalyst particles.

On the other hand, as shown in Part III,[1] significant intraparticle mass transfer resistances can exist in the polymer particle under certain conditions. At the microparticle level, a significant concentration gradient may exist with catalysts of high intrinsic activity, in both slurry and gas phase, depending on the values of catalyst primary crystallite size and the effective diffusion coefficient $D_s$. Another mass transfer resistance that is usually

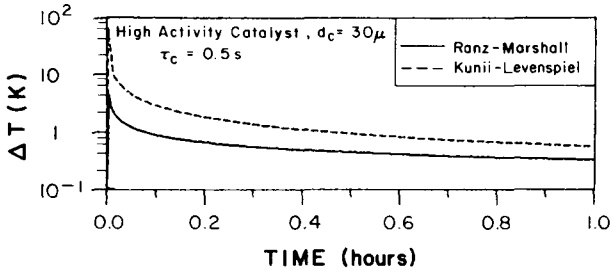


Fig. 41. Comparison of external film heat transfer resistance according to Ranz-Marshall and Kunii-Levenspiel correlations in gas-phase polymerization of ethylene under stirred bed conditions ($u$ = 2 cm/s). High-activity catalyst, particle size $d_c$ = 30 μm, $\tau_c$ = 0.5 s. Average rates (g-g-cat-h); Ranz-Marshall correlation, 3980; Kunii-Levenspiel correlation, 4220.

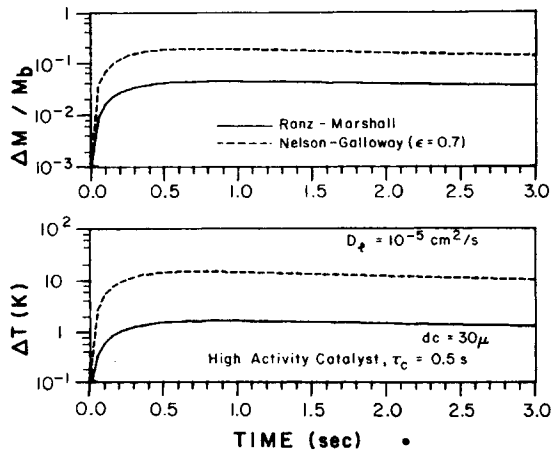


Fig. 42. Comparison of external film heat and mass transfer resistances according to Ranz-Marshall correlation and Nelson-Galloway correlation ($\epsilon = 0.7$) in ethylene slurry polymerization at short times. High-activity catalyst, $d_c = 30$ μm, $\tau_c = 0.5$ s. Large particle diffusivity $D_l = 10^{-5}$ cm²/s. Average rates (g-g-cat-h): Ranz-Marshall correlation, 3800; Nelson-Galloway correlation, 2860.

important in slurry polymerization is diffusion in the pores of the growing macroparticle. By contrast, in gas-phase polymerization, our results indicate that macroparticle concentration gradients would normally be insignificant except for very large catalyst particles. Macroparticle diffusion limitations in slurry polymerization can be experimentally detected by slow acceleration-type rate behavior or by increases in polymerization rate with decreasing catalyst particle size.

As for external film heat transfer resistances in slurry polymerization, the significance of these depends on the catalyst activity and particle size

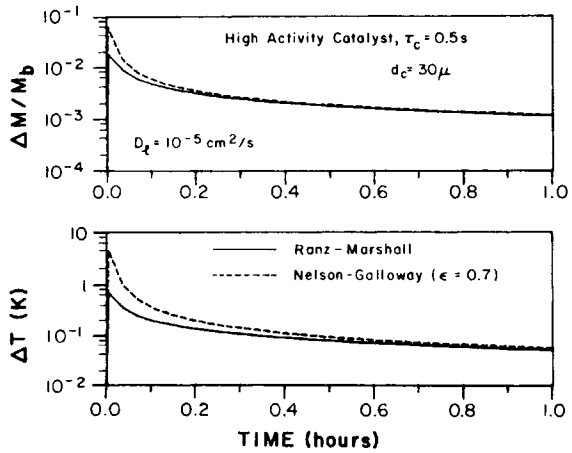


Fig. 43. Comparison of external film heat and mass transfer resistances according to Ranz-Marshall correlation and Nelson-Galloway correlation ($\epsilon = 0.7$) in ethylene slurry polymerization at short times. High-activity catalyst, $d_c = 30$ μm, $\tau_c = 0.5$ s. Large particle diffusivity $D_l = 10^{-5}$ cm²/s. Average rates (g-g-cat-h): Ranz-Marshall correlation, 3800; Nelson-Galloway correlation, 3810.

as well as the correlation used. For large, highly active catalyst particles in concentrated slurry polymerization, large external film temperature gradients are predicted. However, as our simulations show, factors (such as mass transfer resistance) that delay the attainment of full catalyst activity early in the polymerization can mitigate these effects. Thus for slurry polymerization, the external film temperature rise will normally be negligible except very early in the lifetime of polymer particles grown from large highly active catalyst particles.

In gas-phase polymerization, however, the situation is quite different. Although intraparticle temperature gradients are expected to be negligible except for very large particles of high-activity catalyst, external film temperature differences can be large. With high-activity catalyst, particle overheating due to external film resistance can result in a $\Delta T$ of as much as 50–100 K for large catalyst particles very near the beginning of polymerization. These temperatures could result in polymer softening or melting, leading to sticking and agglomeration in the reactor. The results also suggest that the heat transfer resistance in the external film, $\Delta T$, is predicted to fall off rapidly with particle growth. For a 30-$\mu$m high-activity catalyst particle in ethylene gas-phase polymerization under stirred bed conditions, $\Delta T$ is expected to become less than 1 K after a few minutes. However, for a 60 $\mu$m particle, $\Delta T$ is of the order of 10 K for the first minute and is around 1 K even after an hour. Still higher temperature rises are attained at times of a few seconds. However, the interaction between the temperature rise and the speed of particle breakup and/or catalyst activation is very strong, as we have illustrated, making quantitative conclusions difficult. For instantaneous breakup, particle temperatures could reach the melting temperature of the polymer within a fraction of a second in some cases. These conclusions are in agreement with the work of Laurence and Chiovetta,[47] who modeled the particle breakup phenomenon. A point not raised in their work is that the catalyst particle size is an important parameter. A 60-$\mu$m particle might overheat to the melting temperature under conditions in which a 20-$\mu$m particle undergoes a temperature rise of less than 1 K. Hence, in gas-phase polymerization, a catalyst particle size distribution with large particles present could result in agglomeration or fusing problems. Such problems would be most severe immediately after the catalyst is injected into the reactor.

Obviously, control of the catalyst size distribution would help to reduce the agglomeration problems resulting from particle surface overheating. However, very small catalyst particles are not desirable for use in olefin polymerization for other reasons. Catalyst fines are frequently difficult to handle and also are easily blown out of the top of fluidized beds. Also, such small particles may stick to the walls or the tapered upper part of the fluidized bed reactors, where they may overheat due to relatively low fluid velocities. In addition, small catalyst particles are not desirable for achieving the objective of directly producing in the reactor polymer particles that do not require pelletization.

The particle simulations presented illustrate the potential for methods that reduce the *initial* activity of the catalyst to control the overheating problem. Several such methods are in fact described in the patent literature.

For example, separate injection of the catalyst and cocatalyst has been used by BASF[48] in their stirred bed reactor. Other methods, such as mixing the catalyst with particles of polymer prior to injection,[49] prepolymerizing,[50] coating the catalyst with wax,[51] and temporarily deactivating the catalyst,[52] have been referred to in the patent literature. A somewhat different approach is to attempt to inject the catalyst as rapidly as possible,[53] in order to disperse it in the bed of cooler particles. It is probably true that, by judicious application of these methods, overheating and sticking problems can be reduced or eliminated.

It is also worthy of mention that, in gas-phase polymerizations, the fluidized bed may have advantages from the particle-gas heat transfer point of view because of the higher gas velocities. The stirred bed, on the other hand, avoids problems of fines entrainment by keeping the relative velocity low.[54]

There are many practical implications of the results reported here. One may explain the great variety of activation energies reported in the literature, the difficulties sometimes observed in using slurry bench scale studies to predict gas-phase behavior, the increased agglomeration and sticking after a seemingly innocent change in operating conditions, and the apparent differences observed between reaction rate profiles for ethylene and propylene. These and other practical points will be discussed in a future paper.

Table II indicates the relative importance of the various heat and mass transfer resistances discussed in Part III[1] and in this paper.

The authors are grateful to the National Science Foundation and to the following companies for research support: Exxon, duPont, Mobil, and Novacor, Ltd. The authors are also indebted to Dr. Norman Brockmeier and Dr. W. David Smith for helpful comments and references on particle-fluid heat and mass transfer.

## References

1. S. Floyd, K. Y. Choi, T. W. Taylor, and W. H. Ray, *J. Appl. Polym. Sci.*, (submitted 1985).
2. C. McGreavy and N. Rawlings, 4th International Symposium on Chemical Reaction Engineering, Vol. 1, IV-152, Heidelberg, 1976.
3. N. F. Brockmeier and J. B. Rogan, *AIChE Symp. Ser.*, **72**(160), 28 (1976).
4. N. F. Brockmeier, ACS Symposium Series, Vol. 104, J. N. Henderson and T. C. Bouton, Eds., 1979 p. 201.
5. W. E. Ranz and W. R. Marshall, Jr., *Chem. Eng. Prog.*, **48**, 141 (1952).
6. P. H. Calderbank and S. J. R. Jones, *Trans. Inst. Chem. Eng.*, **39**, 363, (1961).
7. K. Wisseroth, *Chem. Zeitung*, **101**, 271 (1977).
8. P. L. T. Brian and H. B. Hales, *AIChE J.*, **15**, 419 (1969).
9. P. A. Nelson and T. R. Galloway, *Chem. Eng. Sci.*, **30**, 1 (1975).
10. P. Harriot, *AIChE J.*, **8**(1), 93 (1962).
11. D. Kunii and O. Levenspiel, *Fluidization Engineering*, Wiley, New York, 1969.
12. J. Y. Oldshue, *Fluid Mixing Technology*, McGraw-Hill, New York, 1983.
13. C. N. Satterfield, *Mass Transfer in Heterogeneous Catalysis*, MIT Press, Cambridge, Massachusetts, 1970.
14. P. Tournie, C. Laguerie, and P. Couderc, *Chem. Eng. Sci.*, **34**, 1247 (1979).
15. P. N. Rowe, *Chem. Eng. Sci.*, **30**, 7 (1975).
16. S. Nagata and M. Nishikawa, Proceedings, First Pacific Chemical Engineering Conference, Pt. 3, Kyoto, 1972, p. 301.
17. K. Y. Choi, Ph.D. Thesis, University of Wisconsin, Madison, 1984.
18. H. Yagi, T. Motouchi, and H. Hikita, *Ind. Eng. Chem. Proc. Des. Dev.*, **23**, 145 (1984).
19. K. Wisseroth, private communication, 1982.

20. J. F. Richardson and J. Szekely, *Trans Inst. Chem. Eng.*, **39**, 212 (1961).
21. H. Littman, R. G. Barile, and A. H. Pulsifier, *I.&E.C. Fund.*, **7**(4), 554 (1968).
22. J. F. Davidson and D. Harrison, *Fluidization*, Academic Press, New York, 1971.
23. E. U. Schlünder, *ACS Symp. Ser.*, **72**, 110 (1978).
24. S. Floyd, Ph.D. Thesis, University of Wisconsin, Madison, 1985.
25. T. Miyauchi, *J. Chem. Eng. Japan*, **4**(3), 238 (1971).
26. D. J. Gunn and J. F. C. De Souza, *Chem. Eng. Sci.*, **29**, 1363 (1974).
27. N. Wakao, K. Tanaka, and H. Nagai, *Chem. Eng. Sci.*, **31**, 1109 (1976).
28. N. Wakao and T. Funazkri, *Chem. Eng. Sci.*, **33**, 1375 (1978).
29. S. Kaguei, B. Shiozawa, and N. Wakao, *Chem. Eng. Sci.*, **32**, 507 (1977).
30. N. Wakao, S. Kaguei, and H. Nagai, *Chem. Eng. Sci.*, **33**, 183 (1978).
31. N. Wakao, S. Kaguei, and T. Funazkri, *Chem. Eng. Sci.*, **34**, 325 (1979).
32. N. Wakao, *Chem. Eng. Sci.*, **31**, 1115 (1976).
33. N. Wakao, Y. Iida, and S. Tanisho, *J. Çhem. Eng. Japan*, **7**(6), 438 (1974).
34. N. Wakao, *Kagaku Kogaku*, **21**(1), 41 (1957).
35. N. Wakao, *Chem. Eng. Sci.*, **32**, 1261 (1977).
36. N. Wakao, S. Kaguei, and B. Shiozawa, *Chem. Eng. Sci.*, **32**, 451 (1977).
37. J. Shen, S. Kaguei, and N. Wakao, *Chem. Eng. Sci.*, **36**, 1283 (1981).
38. T. Miyauchi, H. Kataoka, and T. Kikuchi, *Chem. Eng. Sci.*, **31**, 9 (1976).
39. T. Miyauchi, K. Matsumoto, and T. Yoshida, *J. Chem. Eng. Japan*, **8**(3), 228 (1975).
40. P. Chen and O. C. T. Pei, *Can. J. Chem. Eng.*, **62**, 469 (1984).
41. D. Kunii and M. Suzuki, *Int. J. Heat Mass Transfer*, **10**, 845 (1967).
42. H. Martin, *Chem. Eng. Sci.*, **33**, 913 (1978).
43. P. Tournie, C. Laguerie, and J. P. Couderc, *Chem. Eng. Sci.*, **32**, 1259 (1977).
44. K. N. Kettenring, E. L. Manderfield, and J. M. Smith, *Chem. Eng. Prog.*, **46**(3), 139 (1950).
45. F. A. Zenz and D. F. Othmer, *Fluidization and Fluid-Particle Systems*, Reinhold, New York, 1960.
46. V. A. Borodulya, V. G. Ganzha, and A. I. Podberezsky, in *Fluidization*, J. R. Grace and J. M. Matsen, Eds., Plenum Press, New York, 1980, p. 201.
47. R. L. Laurence and M. G. Chiovetta, *Proceedings Berlin Workshop on Polymer Reaction Engineering*, Edited by K. H. Reichert and W. Geisler, Eds., Hanser Verlag, Munich, October, 1982, p. 73.
48. U.S. Patent 3,652,527 (1972) to BASF.
49. U.S. Patent 3,772,261 (1973) to Scholven-Chemie.
50. U.S. Patent 3,922,322 (1975) to Naphthachemie.
51. U.S. Patent 4,200,715 (1980) to Gulf.
52. U.S. Patent 4,130,699 (1978) to Standard Oil of Indiana.
53. U.S. Patent 3,876,602 (1975) to Union Carbide.
54. U.S. Patent 3,300,457 (1967) to BASF.

Received June 24, 1985
Accepted August 24, 1985